Vacuum 169 (2019) 108928

Contents lists available at ScienceDirect

Vacuum

journal homepage: www.elsevier.com/locate/vacuum

Microproperties and interface behavior of the BAg25TS brazed joint

Liangliang Zhang[a,b], Hua Yu[a,b], Jia Ma[c], Sujuan Zhong[c], Yongtao Jiu[c], Shizhong Wei[a,b,*], Weimin Long[c,**], Alex A. Volinsky[d]

[a] School of Material Science & Engineering, Henan University of Science and Technology, Luoyang, 471003, China
[b] National Joint Engineering Research Center for Abrasion Control and Molding of Metal Materials, Luoyang, 471003, China
[c] Zhengzhou Research Institute of Mechanical Engineering Co. Ltd., Zhengzhou, 450000, China
[d] Department of Mechanical Engineering, University of South Florida, Tampa, FL, 33620, USA

ARTICLE INFO

Keywords:
Flux-core solder
Induction brazing
Mechanical properties
Microstructure
Element diffusion

ABSTRACT

A joint with a Q235A steel Bundy tube as the base metal induction brazed with a new type of BAg25TS flux-cored solder, and a butt joint and lap brazing test were carried out. The temperature range of the solid-liquid phase line of the brazed joint, wettability on the base metal, microstructure, element distribution and diffusion of the joint, and mechanical properties of the joint were studied using a differential scanning calorimeter, thermal balance, field emission scanning electron microscope, energy dispersive spectroscopy, tensile testing and microhardness measurements. The solid-liquid line range of the flux-core solder is 775.7–801.4 °C and the spread area of the solder on the base metal is the largest at 850 °C. Additionally, the joint brazed with this flux-core solder has no microcracks, and a secondary phase appears, which is mainly composed of an interface Cu-rich and Ag-rich phases. The Ag element in the joint is distributed along the grain boundaries through intergranular infiltration of the Fe. Furthermore, the pinning effect optimizes the tensile and shear strength of the joint, and the fracture surface of the joint indicates a ductile fracture. In addition, the microhardness of the brazed joint is high on the left side, while it is low on the right side due to the difference in the element distribution between the interfaces of the Cu-rich phase. Remarkably, the inhomogeneous distribution was caused by the different degree of undercooling between the two sides of the joint.

1. Introduction

Silver-based solder is widely used in welding low-carbon, stainless and low-alloy steels, high-temperature nickel-based alloys, copper-based alloys and other materials due to its low melting point, high strength, good electrical and thermal conductivity, along with good corrosion resistance [1,2]. Particularly, silver-based brazing solder is often used in the connection of Bundy tubes in household appliances, particularly refrigerators. The brazing temperature is lower than the liquid-line temperature of the base metal, and the deformation of the joint is small. Also, the silver-based solder has excellent wettability and low melting point, which has little effect on the properties of the matrix [3,4]. However, during brazing, the main forms of brazing alloy/flux composite application are: solid brazing alloy dipping flux, solid brazing alloy and paste brazing alloy synergistic addition, paste brazing alloy, coating brazing alloy and so on. Among them, the solid solder dip brazing agent is the most commonly used method of manual brazing. However, this method of discrete-adding brazing material and brazing agent increases the working procedure and operation time before the first welding and adds a variable in the brazing process, which affects the consistency and stability of welding. Meanwhile, in order to ensure the quality of brazing, excessive flux has to be added, which not only pollutes the air, endangers the health of operators, but also causes flux waste. The synergistic adding of solid solder and paste flux has high cost and great performance fluctuation. In order to improve the process, an adhesive is needed to be added. During the brazing process, the adhesive used in the burning produces smoke and affects the health of operators. Atomization powder is needed in the preparation of solder paste, which leads to the high oxygen content of the solder. The solder filler metal has disadvantages, such as moisture absorption, easy breakage, and difficulty in storage and transportation. The flux-core solder is used to realize the compact wrapping of flux without adding additional adhesive. At the same time, the flux hidden in the core is not exposed to the external environment and is not affected by the field equipment, storage and transportation conditions [5,6]. Fortunately, a new type of silver-based flux-core solder meets the requirements of

* Corresponding author. School of Material Science & Engineering, Henan University of Science and Technology, Luoyang, 471003, China.
** Corresponding author.
E-mail addresses: wsz@haust.edu.cn (S. Wei), volinsky@usf.edu (A.A. Volinsky).

https://doi.org/10.1016/j.vacuum.2019.108928
Received 14 August 2019; Received in revised form 6 September 2019; Accepted 6 September 2019
Available online 07 September 2019
0042-207X/

green manufacturing and is suitable for automatic and intelligent welding technology. Domestic research shows that compared with traditional solder, the flux-cored solder improves the production efficiency and ensures the brazing quality [7]. The content of silver in the silver-based flux-core solder is determined and the application of the flux-cored solder in Bundy tubes are discussed in this paper. Compared with high-frequency induction brazing, vacuum brazing has its own unique advantages. The base material will not oxidize in a vacuum. Therefore, under the condition of vacuum brazing, the brazing process does not require adding the flux. This not only saves the experiment cost but also the flux will not remain in the joint, thus improving the corrosion resistance and mechanical properties of the joint. The solder has good wettability and fluidity in a vacuum environment, so it can weld complex or precise joints of brazing joints. However, the equipment involved in vacuum brazing is complex and expensive, making it difficult to automate production. On the other hand, high-frequency induction brazing has fast heating speed, small heating area and low influence on base metal heat in the brazing process. The high-frequency induction brazing equipment can achieve accurate heating control and improve production efficiency by realizing automatic production. The automatic production of high-frequency induction brazing equipment and flux-core brazing filler metal not only improves the welding efficiency but also reduces the flux usage and improves the corrosion resistance and mechanical properties of joints compared with traditional brazing because of the reasonable proportion of flux-core brazing filler metal and flux [8,9].

The Degussa and Umicore companies and the Xue Songbai, Long Weimin and other research groups have developed a series of high-silver and low-silver solders with 16 wt% and 65 wt% silver content, respectively [10,11]. However, the element diffusion, element distribution and mechanical properties of a joint brazed with the low-silver flux-cored solder with a Q235A steel Bundy tube as the base metal have not been systematically studied. For this reason, the solid-liquid line range, wettability, microstructure, element diffusion and element distribution of a joint with Q235A steel Bundy tube as base metal and a new type of low silver-based flux-core solder are studied in this paper. Furthermore, the mechanical properties are also analyzed and studied.

2. Materials and methods

A Q235A steel matrix sample was used in the wetting experiment with the 40 mm × 40 mm × 3 mm dimensions and for the Bundy tube experiments the dimensions were 70 mm × 20 mm × 3 mm. The chemical compositions of the Q235A steel, as well as a new type of flux-cored solder named BAg25TS, are listed in Table 1.

Before induction welding, the core material of the solder was subjected to differential thermal analysis, and the melting temperature was determined. Thus, the wettability of the solder on the base material was determined, along with the optimal wetting temperature. The welding joint was in the form of a butt joint and a lap joint. The joint overlap length was 5 mm, and the base material was fixed on a special fixture in the form of an overlapping length and butt joint. The clamp is shown in Fig. 1. After the welding, the joint was heated for 10 s, and then air-cooled. The tensile strength and shear strength of the joint were tested using a Shimadzu AG-I250KN precision universal tensile testing machine, and the interface morphology of the joint was observed by using a JSM-560 LV scanning electron microscope (SEM). The element diffusion and the composition of the solid solution were determined by using energy dispersive spectroscopy (EDS) and a field emission scanning electron microscope.

Table 1
Composition of matrix materials and solder in wt.%.

Materials	Fe	C	Mn	Si	Ag	Cu	Zn	Sn	Other
Q235A	Base	0.14–0.22	0.30–0.65	≤0.30	–	–	–	–	≤0.095
BAg25TS	–	–	–	–	25	39	34	1	≤0.1

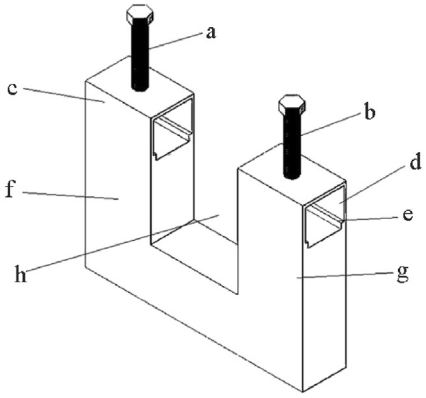

Fig. 1. Schematic diagram of the high-frequency induction welding fixture: (a, b) Compression bolts; (c) Second u-bracket; (d) First u-bracket; (e) Steps; (f) Second stand; (g) First stand and (h) u-slots.

3. Results and discussion

3.1. DSC analysis of the solder

In the experiment, 10 mg of the material were used, and the heating rate was 10°/min. Fig. 2 shows the differential scanning calorimetry (DSC) and thermogravimetric (TG) curves of the BAg25TS solder alloy. The solder has two endothermic reaction peaks at 794.5 °C and 947 °C and the corresponding temperature intervals are 775.7–801.4 °C and 936.7–972 °C respectively. At 801.4 °C, the melting process corresponds to the first endothermic reaction peak because there is no mass change in the melting process of the solder alloy. The difference between the experimentally determined melting temperature range and the melting temperature range in the phase diagram is obvious, and the difference is related to the experimental conditions and a change in the elemental composition [12]. The melting temperature range of the solder alloy is small, which indicates that the molten solder has good flow spreading in the brazing seam [13].

3.2. Analysis of the wetting spread of solder

The experiment was conducted to determine the spreading performance of the solder core material at 800 °C, 825 °C, 850 °C, and 875 °C, shown in Fig. 3. The solder spreads well on the Q235 base metal. After

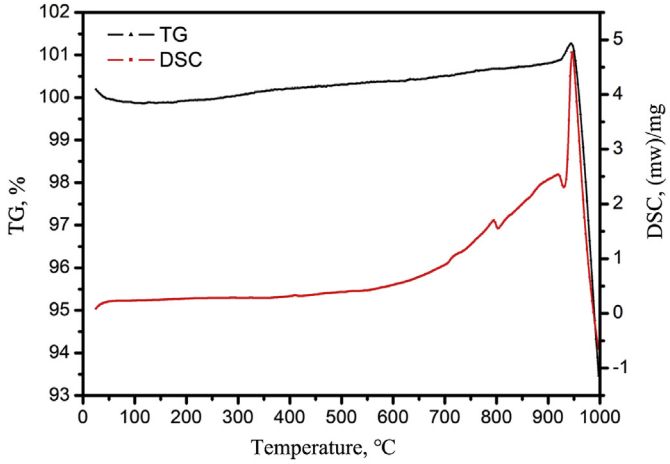

Fig. 2. DSC and TG curves of the BAg25TS filler metal.

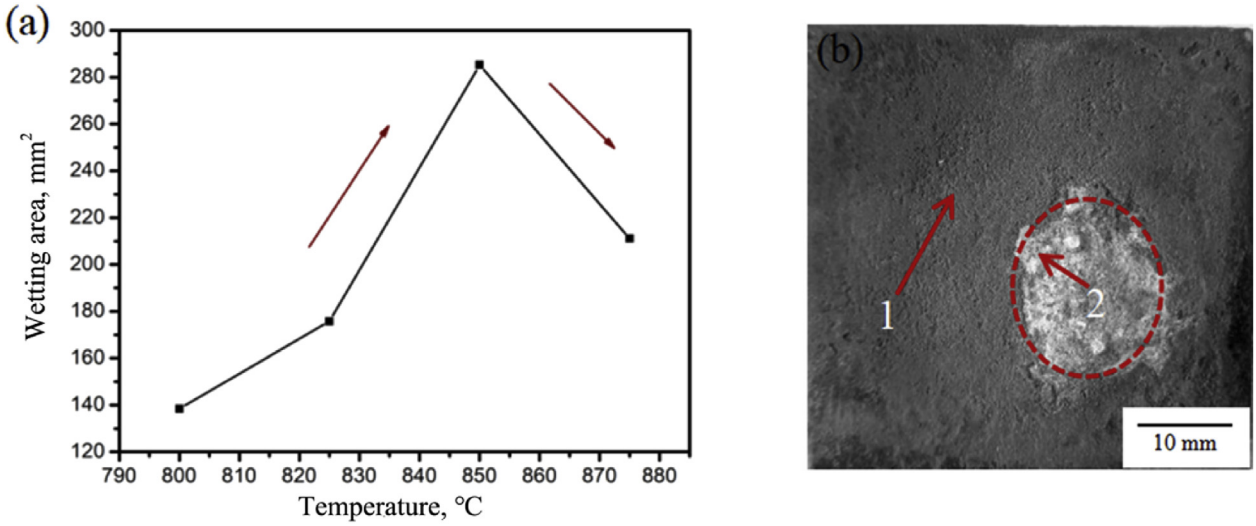

Fig. 3. (a) Wetting area of BAg25TS solder at different temperatures; (b) wetting and spreading morphology of solder on a steel plate at 800 °C.

wetting on the base metal, the solder shows ring regions 1 and 2 in Fig. 3. Furthermore, the ring region 1 is formed by low melting point impurities and the oxide film cleaned by the flux, and the ring zone 2 is the morphology of the spreading liquid solder under the oxide film when the solder begins to melt [14]. At 850 °C, the spreading area of the flux-core solder is the largest, indicating that the spreading and wettability are the best at this temperature. However, when the temperature continues to rise, the spreading area decreases, and the wettability becomes worse. The main reason is that the volatilization of the flux accelerates with temperature. As the solder is not melted, the flux has failed, and the base metal is substantially oxidized resulting in the poor wettability of the flux-core solder.

3.3. Interface structure and element diffusion of the welded joint

Fig. 4 shows the interface structure of the induction brazed joint. The flux-core solder has good wetting with the base metal and thereby forming a dense interfacial bond. No microcracks, slag clamping or secondary phases were found. The uniform fusion line between the weld and the base metal indicates that the Q235A steel and solder can produce a metallurgical bond [15]. The brazed joint is composed of the three regions, namely, the brazing zone, the interface zone, and the base metal. It can be seen from the microstructure of the brazing zone that the solder side and the brazing zone in the interface zone are mainly composed of a clustered gray-black phase and a needle-like gray-white phase distributed along the grayish-black phase. The EDS analysis results of the related positions of the brazed joint are listed in Table 2, which indicate that the clustered gray-black phase and the needle-like gray-white phase in the joint are Cu-rich and Ag-rich phases, respectively [16]. The root positions are a, b, d, f, g, h, i, and j in

Table 2
Results of EDS analysis of BAg25TS brazed joints.

Point	W(Fe)	W(C)	W(Ag)	W(Cu)	W(Zn)	W(other)	Deduced phases
a	91.7	8.3	–	–	–	–	Fe 3c + α-Fe
b	–	–	29.5	45.9	29.5	–	Interface-rich Cu phase (IRCP)
c	3.5	9.6	13.4	51.6	22.0	–	IRCP
d	–	–	60.1	18.7	21.2	–	IRAP
e	–	–	52.5	16.3	25.7	5.6	Brazing-rich Ag phase (BRAP)
f	–	–	15.1	57.2	27.7	–	BRCP
g	–	–	14.8	58.7	26.5	–	BRCP
h	–	–	57.3	16.2	19.9	6.6	BRAP
i	–	–	15.2	55.6	29.2	–	BRCP
j	–	–	52.8	18.6	21.6	7.1	BRAP
k	–	–	25.2	50.5	24.3	–	–
m	–	–	52.6	22.4	25	–	–

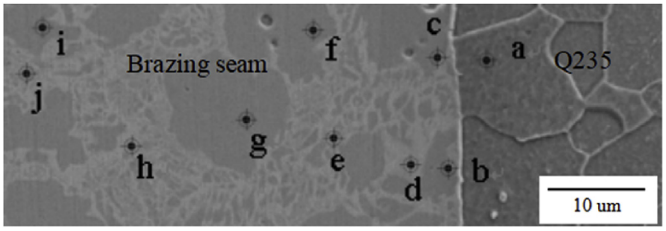

Fig. 5. EDS analysis of the BAg25TS brazed joint at 850 °C.

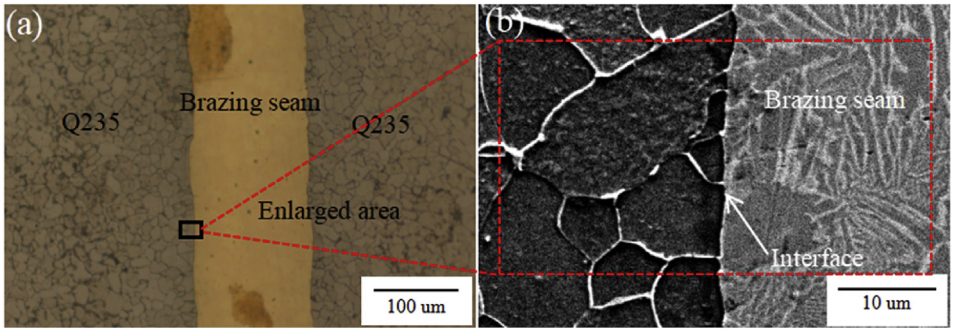

Fig. 4. The microstructure of BAg25TS brazed joint at 850 °C: (a) optical image; (b) SEM image.

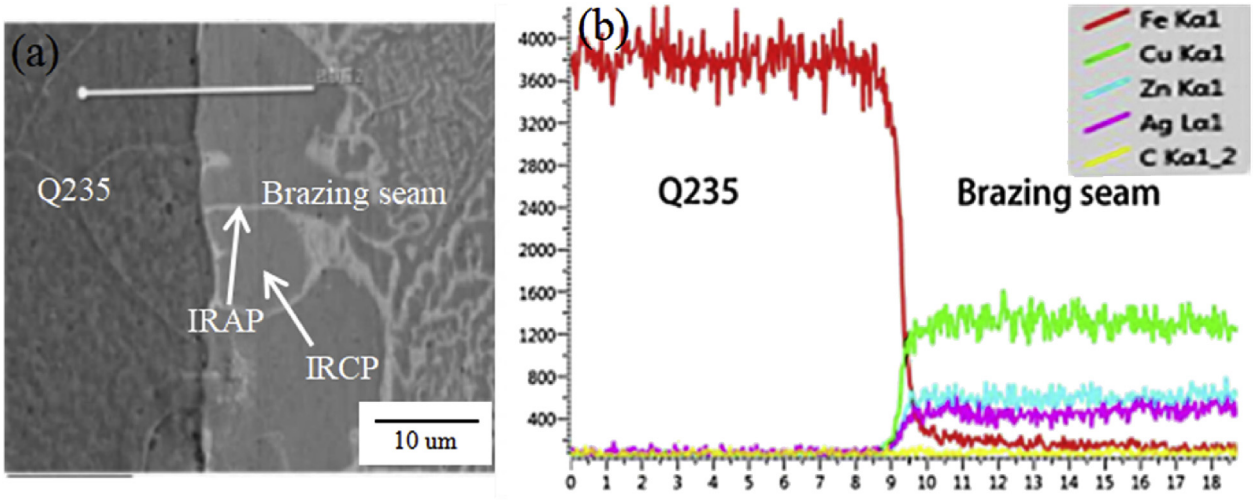

Fig. 6. (a) SEM image of the BAg25TS brazed joint showing the location of the EDS line scan, (b) EDS line scan analysis of the BAg25TS brazed joint at 850 °C.

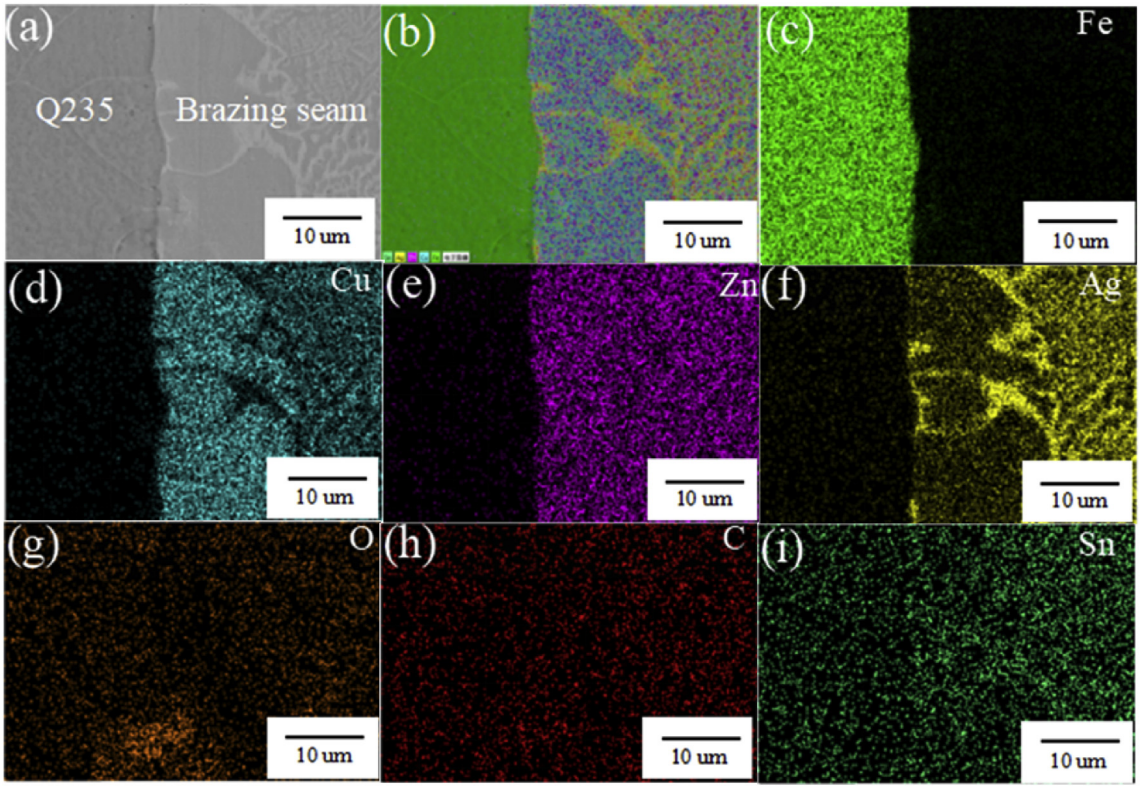

Fig. 7. (a) SEM image of the interface side of the BAg25TS brazed joint, (b) combined elemental map and element distribution maps of (c) Fe, (d) Cu, (e) Zn, (f) Ag, (g) O, (h) C, (i) Sn.

Table 3
Tensile and shear strength of the BAg25TS brazed joint.

Butt joint				5 mm lap joint			
Maximum load, kN	12.102	11.945	12.906	Maximum load, kN	11.13	11.99	11.26
Tensile strength, MPa	201.693	199.09	215.1	Shear strength, MPa	111.2	119.8	114.3

Table 4
Tensile and shear strength of the BAg30T brazed joint.

Butt joint				5 mm lap joint			
Maximum load, kN	9.76	10.67	10.39	Maximum load, kN	8.74	7.92	8.25
Tensile strength, MPa	162.63	177.87	173.18	Shear strength, MPa	87.4	79.22	82.55

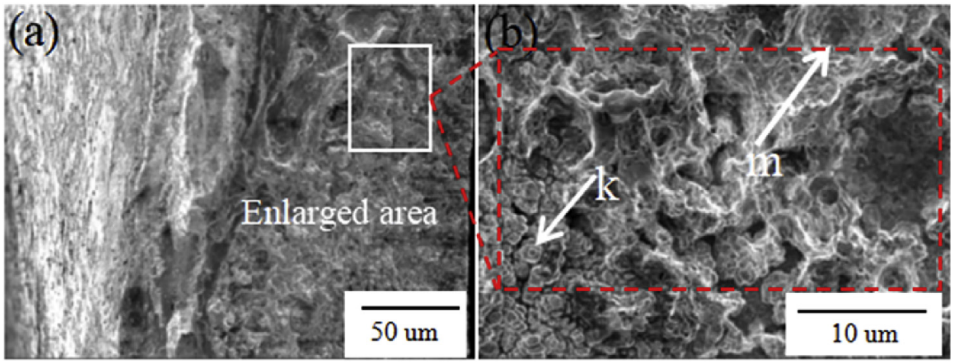

Fig. 8. Tensile fracture morphology of the BAg25TS brazed butt joint: (a) low magnification and (b) high magnification SEM images.

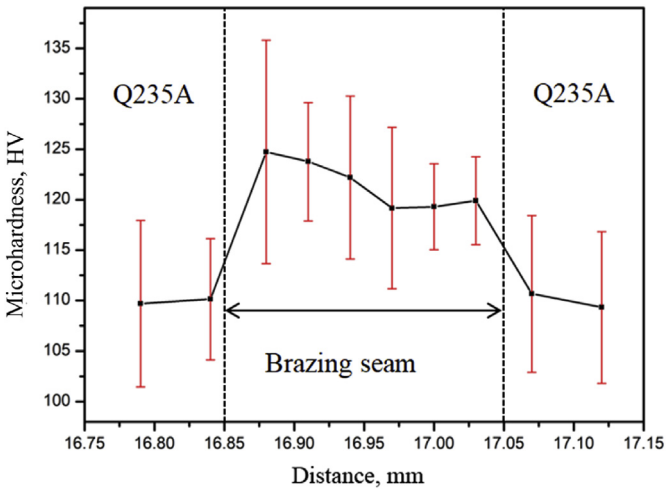

Fig. 9. Microhardness of the BAg25TS brazed joint.

Fig. 5. According to the positions of the two phases in the brazed joint, the Cu-rich and Ag-rich phases in the interface area are referred to as the interface-rich Cu phase (IRCP) and interface-rich Ag phase (IRAP), respectively. The Cu-rich and Ag-rich phases in the brazing seam area are referred to as the brazing-rich Cu phase (BRCP) and the brazing-rich Ag phase (BRAP), respectively.

Fig. 6 shows the scan of the Cu-rich phases in Fig. 4(b). The elements in the brazing zone, at the interface and in the base metal have diffused together. The amount of Fe element in the base metal decreases at a certain distance from the interface, and the Cu element in the interface brazing seam zone also begins to decrease when it is at a certain distance from the interface. The Ag and Zn elements have an obvious diffusion trend into the base metal, and the Cu element concentration decreases very quickly at the interface, followed by Zn and Ag. According to the Cu–Fe and Fe–Zn phase diagrams, it can be seen that at a high-frequency induction brazing temperature, Ag does not form a solid solution with Fe in the base metal, while Zn has a high solid solubility in Fe, and Cu has low solid solubility in Fe.

Fig. 7 illustrates the diffusion results of the base metal, interface and brazing elements at the induction brazing temperature. Ag accumulates along the Cu-rich grain boundary in the interface brazing zone. Since Ag infiltrates into Fe through the interface along the grain boundaries of the base metal, it can be seen that Ag is distributed along the Fe grain boundaries, and the pinning effect caused by the corresponding grain boundary penetration is beneficial to the mechanical properties of the brazed joint [17]. The concentration of copper in the copper-rich phase on the brazing seam side is the highest, and with increasing distance in the brazing seam zone, the composition of the Cu decreases gradually with distance. In the Fe base metal, Cu is distributed along the grain boundaries, and a solid solution with Fe occurred. Zn can not only dissolve with Fe on the base metal side but also distribute along the Fe grain boundaries. After the Fe in the base metal diffuses through the interface, it is mainly distributed on the brazing side of the interface. Moreover, with increasing distance, the composition decreases gradually. The concentration of trace Sn element in the copper-rich phase on the interface brazing side is lower than in the Cu-rich phase in the brazing zone, which is mainly due to the low melting point of Sn, undercooling at the interface after brazing, high liquid-line temperature of the rich Cu clusters, preferential nucleation at the interface and growth at the vertical interface [18].

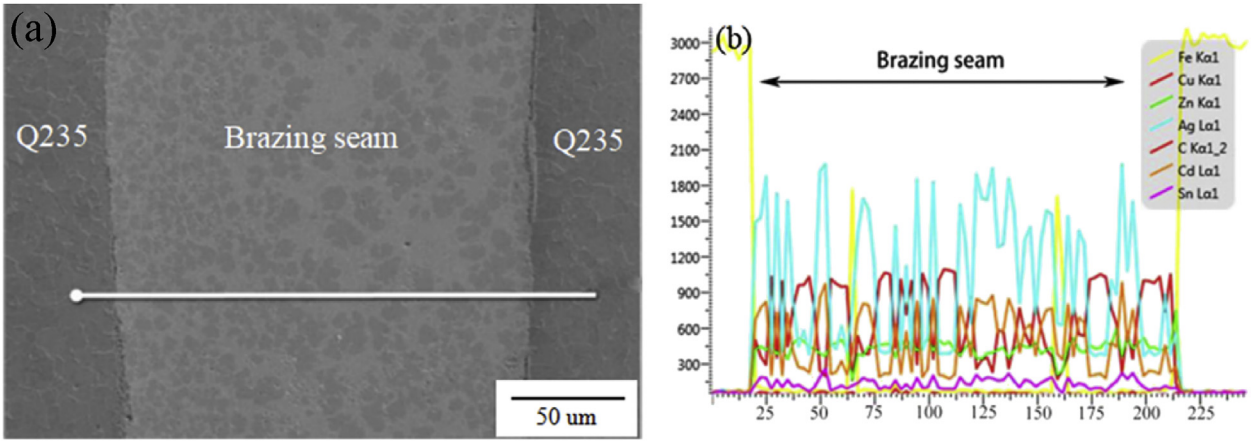

Fig. 10. (a) SEM image of the EDS line scan area, (b) EDS elemental line profiles of the BAg25TS brazing seam.

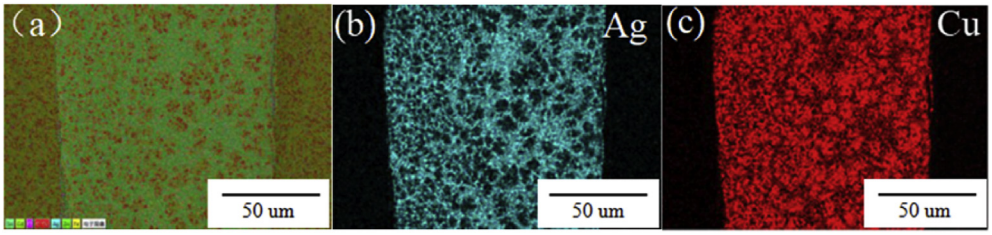

Fig. 11. EDS element distribution maps of the BAg25TS brazing seam: (a) combined map, (b) Ag and (c) Cu.

3.4. Mechanical properties of brazed joint

At the above optimal wetting temperature, the brazing lap length is 5 mm. The tensile test was carried out according to the GB/T 228.1–2010 standard. When the tensile test was carried out, the specimens prepared with the two brazing methods were broken on the brazing seam, and the shear strength and tensile strength are listed in Table 3. Table 4 shows the tensile strength and the shear strength of the BAg30T brazing joint at 850 °C. The mechanical properties of the joints brazed with BAg25TS flux-core solder are significantly better than the those brazed with the BAg30T flux-core solder.

The tensile strength of the solder is 58.84% of the base metal, and the shear strength of the solder is 56% of the tensile strength of the solder. The allowable shear stress, τ, and the allowable yield stress were calculated using the following equation:

$$\tau = 0.56\sigma \quad (1)$$

Because $0.5 \leq 0.56 \leq 0.7$, the brazed joint with the new type of low-silver flux-core brazed joint experienced ductile fracture during the tensile test [19].

Fig. 8 shows the fracture morphology of the Q235A steel induction brazed butt joint after tensile fracture at 850 °C. The macroscopic morphology of the fracture surface is shown in Fig. 8(a), and the tensile fracture surface is relatively smooth, which also shows that the brazing solder and the base metal in the interface zone achieve good metallurgical bonding. The fracture morphology is shown in Fig. 8(b), which contains dimples, indicating that the joint experienced ductile fracture. The dimples are either large and deep or small and shallow. During the tensile testing of the specimen, a large and deep dimple was formed in the large part of the weld under stress, while a small and shallow dimple was formed in the small part of the weld under stress. The small and shallow dimples were analyzed by EDS, and the composition at the point labeled g was determined. The content of Ag is high at the g point, and there are F and K residuals from the flux. The residual flux in the brazing joint corrodes and obstructs the connection between the base material and the brazing joint welding interface so that a firm and good joint should be formed in the brazing process, and the interface of the brazing joint with residual flux in the stretching process produces crack source [20]. It can be inferred that the crack initiation source of the brazed joint is the interface between the Cu-rich and Ag-rich phases, and the crack propagates along the Ag-rich phase [21,22].

As shown in Fig. 9, the hardness of the BAg25TS brazed joint is higher than the matrix. The highest hardness is 125.8 HV, the microhardness of the sample fluctuates around 109 HV, and the microhardness of the brazed joint is higher than both base metals. In the brazed joint area, the microhardness of the right side is higher than the left brazing seam, so EDS analysis of the whole brazed joint was carried out.

It can be clearly observed from Fig. 10(a) that the number of gray-black cluster interface-rich Cu phases and Cu-rich phases in the brazing seam zone of the left interface is significantly higher than on the right side of the whole brazing zone. Therefore, the EDS results and Fig. 11 surface scanning results of the brazing seam confirm this view. It is confirmed that after high-frequency induction brazing, undercooling occurs at the brazing interface, and the molten solder is cooled and solidified first. Because the Cu-rich phase in the liquid filler metal has a high liquid phase line, the core is formed first and the vertical interface is long under the condition of the subcooling degree of the brazing joint interface. In the induction brazing process on the left side of the base material, in order to improve the heat conduction efficiency, there is a steel plate, so there is more time for the Cu-rich phase on the left side of the brazing joint to nucleate and grow compared with the Cu-rich phase on the right side of the interface. Because of the different cooling rate, the grain on the side of the cushioned steel plate cooled at a relatively slow rate and underwent relatively sufficient normalizing to refine the microstructure. Finally, on the right side of the brazing seam, the Ag-rich phase with low liquid line accounts for more, and the grain size is large, which leads to the higher microhardness on the left side than on the right side of the brazing seam [23,24] .

4. Conclusions

(1) According to the DSC results obtained from the BAg25TS flux-core material, there are two heat absorption peaks, and the corresponding peak temperature is 775.7–801.4 °C and 936.7–972 °C. The temperature of the low-silver flux-core material-solid liquid-phase line is 775.7–801.4 °C, the solid-liquid section is 25.7 °C, and the melting temperature range is narrow.

(2) When the BAg25TS flux-core solder is wetted and spread on the Q235A base metal, it forms 1 and 2 ring regions, and the wetting spreading area is the largest at 850 °C. The wetting spreading area, as well as the wettability of the solder, decrease with temperature.

(3) In the welding joint, the clustered gray-black Cu-rich phase and the acicular off-white Ag-rich phase were distributed along the Cu-rich phase. When the elements in the graphite material diffuse to the parent material through the interface, the rate of intergranular penetration of the Cu element decrease is the fastest, and that for the Ag element is the slowest. The Fe element in the base material is mainly distributed on the interface seam side by diffusion, and the Ag element is mainly distributed at the grain boundary of the base material. The Cu and Zn and Fe form solid solutions and are distributed at the grain boundaries.

(4) The tensile strength and shear strength of the welded joint are 173.18 MPa and 114.3 MPa, respectively, at 850 °C and 10 s. The fracture mechanism of the joint is mainly ductile, and the source of the fracture is the interface between the Cu-rich phase and the Ag-rich phase, and there is a flux residue present.

(5) The microhardness of the weld is obviously higher than the base metal. The highest hardness of the brazed joint is 125.8 HV at 200 g, and the microhardness of base metal is 109 HV at 200 g. The microhardness of the brazing seam on the left side is higher than that on the right side.

Acknowledgments

The authors gratefully acknowledge funding from the Key Projects of Strategic International Scientific and Technological Innovation Cooperation.(grant no. 2016YFE0201300).

References

[1] M. Jia, L. Weimin, H. Peng, B. Li, X. Peng, W. Mingfang, Effect of gallium addition on microstructure and properties of Ag-Cu-Zn-Sn alloys, China Weld. 24 (3) (2015) 6–10.

[2] X. Wang, L. Shuai, P. Jin, Corrosion behaviors of 316LN stainless steel joints brazed with Sn-plated silver filler metals, Int. J. Mod. Phys. B (2018) 1850198.

[3] A. Wierczyńska, D. Fydrych, G. Rogalski, Diffusible hydrogen management in underwater wet self-shielded flux cored arc welding, Int. J. Hydrogen Energy 42 (38) (2017) 24532–24540 S0360319917331397.

[4] R. Sun, Y. Zhu, W. Guo, P. Peng, L. Li, Y. Zhang, Microstructural evolution and thermal stress relaxation of Al 2 O 3/1Cr18Ni9Ti brazed joints with nickel foam, Vacuum 148 (2017) S0042207X1731240X.

[5] S. Huang, W.M. Long, Q.B. Lu, Y.T. Jiu, S.J. Zhong, Research on the corrosion resistance of Cu-Al joints brazed with flux-cored Zn-2Al filler metal, Mater. Res. Express 6 (5) (2019) 2053.

[6] Y. Wang, Z.Z. Duan, G. Chen, Q.Y. Jiang, W. Dong, K. Lei, Effects of brazing temperature on microstructure and properties of interface between cBN and Co-based active filler metals, Vacuum 145 (2017) 30–38 S0042207X16304304.

[7] T. Watanabe, A. Yanagisawa, T. Sasaki, Development of Ag based brazing filler metal with low melting point, Sci. Technol. Weld. Join. 16 (6) (2011) 502–508.

[8] J. Cao, L.X. Zhang, H.Q. Wang, Effect of silver content on microstructure and properties of brass/steel induction brazing joint using Ag-Cu-Zn-Sn filler metal, J. Mater. Sci. Technol. 27 (4) (2011) 377–381.

[9] Y. Wang, Y.T. Zhao, Z.W. Yang, D.P. Wang, Microstructure, residual stress and mechanical properties of Al2O3/Nb joints vacuum-brazed with two Ag-based active fillers, Vacuum 158 (2018) 14–23.

[10] C. Ma, S. Xue, B. Wang, Study on novel Ag-Cu-Zn-Sn brazing filler metal bearing Ga, J. Alloy. Comp. 688 (2016) 854–862.

[11] D. Schnee, G. Wiehl, S. Starck, C. Kevin, Development of Ag-Cu-Zn-Sn brazing filler metals with a 10 weight-% reduction of silver and same liquidus temperature, China Weld. (4) (2014) 25–31.

[12] V.K. Beura, V. Xavier, T. Venkateswaran, K. Kulkarni, Interdiffusion and microstructure evolution during brazing of austenitic martensitic stainless steel and aluminum-bronze with Ag-Cu-Zn based brazing filler material, J. Alloy. Comp. 740 (2018) 852–862 S0925838818300446.

[13] J.L. Qi, Z.Y. Wang, J.H. Lin, T.Q. Zhang, A.T. Zhang, J. Cao, Graphene-enhanced Cu composite interlayer for contact reaction brazing aluminum alloy 6061, Vacuum 136 (2016) 142–145.

[14] R. Koleňák, M. Chachula, Characteristics and properties of Bi-11Ag solder, Solder. Surf. Mt. Technol. 25 (2) (2013) 68–75.

[15] M. Chaoli, S. Xue, W. Bo, Study on novel Ag-Cu-Zn-Sn brazing filler metal bearing Ga, J. Alloy. Comp. 688 (2016) 854–862.

[16] J.G. Liu, C.W. Tan, L.J. Wu, X.Y. Zhao, Z.Q. Zhang, Butt laser welding-brazing of AZ31Mg alloy to Cu coated Ti-6AL-4V with AZ92 Mg based filler, Opt. Laser. Technol. 117 (2019) 200–214.

[17] S.P. Dimitrijevi, D. Manasijevi, Kamberovi, S.B. Dimitrijevi, M. Mitri, M. Gorgievski, Experimental investigation of microstructure and phase transitions in Ag-Cu-Zn brazing alloys, J. Mater. Eng. Perform. 27 (4) (2018) 1570–1579.

[18] P. Xue, Y. Zou, P. He, Y. Pei, H. Sun, C. Ma, Development of low silver AgCuZnSn filler metal for Cu/steel dissimilar metal joining, Metals 9 (2) (2019).

[19] M.C. Troparevsky, J.R. Morris, M. Daene, Beyond atomic sizes and hume-rothery rules: understanding and predicting high-entropy alloys, J. Occup. Med. 67 (10) (2015) 2350–2363.

[20] Z. Lai, S. Xue, X. Han, L. Gu, W. Gu, Study on microstructure and property of brazed joint of AgCuZn-x(Ga, Sn, in, Ni) brazing alloy, Rare Metal Mater. Eng. 39 (2010) 397–400.

[21] J. Yang, H. Lee, A.R. Choi, K.H. Park, J.H. Ryu, E.J. Oh, Comparison of allergen-specific IgE levels between Immulite 2000 and ImmunoCAP systems against six inhalant allergens and ten food allergens, Scand. J. Clin. Lab. Investig. (2018) 1–7.

[22] C. Xia, W. Sun, Y. Zhou, X. Xu, Thermal fatigue damage and residual mechanical properties of W-Cu/Ag-Cu/1Cr18Ni9 brazed joint, J. Alloy. Comp. 741 (2018) 155–160.

[23] C. Ma, S. Xue, B. Wang, J. Wang, A. Hu, Effect of Ce addition on the microstructure and properties of Ag17CuZnSn filler metal, J. Mater. Eng. Perform. 26 (7) (2017) 3180–3190.

[24] Q. Miao, W. Ding, Y. Zhu, Z. Chen, Y. Fu, Brazing of CBN grains with Ag-Cu-Ti/TiX composite filler—Part I: effect of TiX particles on microstructure and strength of bonding layer, Mater. Des. 98 (2016) 243–253.